DOI: 10.61782/fa.2025.0941

FORUM ACUSTICUM
EURONOISE 2025

OPTIMIZATION ALGORITHM FOR AOTF PARAMETER CHARACTERIZATION

Jurgen Vanhamel[1,2*] **Aleksandr Pavlov**[1] **Samuel Dupont**[3]
[1] TU Delft - Faculty of Aerospace Engineering, Kluyverweg 1, 2629 HS Delft, The Netherlands
[2] Electronic Circuits and Systems, KU Leuven, Kleinhoefstraat 4, 2440 Geel, Belgium
[3] l'Université Polytechnique Hauts-de-France (UPHF), IEMN – Campus Mont Houy – Cedex 9, 59313 Valenciennes, France

ABSTRACT

One of the main challenges for users applying an AOTF as a commercial off-the-shelf component for optical wavelength filtering, is the lack of detailed manufacturing information on critical parameters. Information such as diffraction angles, the precise RF driving frequencies required for momentum-matching conditions, as well as the data for each wavelength across a certain optical spectrum is not always easily available. To obtain this information, users must perform physical tests to configure the optimal frequencies, diffraction angles, and incidence angles for each wavelength of interest which is labor-intensive and costly.
This research uses an optimization algorithm applied to an analytical model which can characterize key angles related to the AOTF's crystallographic axis, such as the crystallographic axis angle θ_c, the tilt-angle α, as well as facet inclination angles β and γ. First, diffraction testing on an AOTF is done, by recording both output ray angles and the momentum-matching frequency. Then the optimization algorithm is chosen and applied to the analytical model to determine the optimal parameters for θ_c, α, γ, and β. With these parameters, the AOTF's behavior can be extrapolated to multiple wavelengths, which not only saves time, but also enables more versatile planning of optical setups..

Keywords: *AOTF, optimization model, analytical model.*

1. INTRODUCTION

Acousto-Optic Tunable Filters (AOTFs) make use of acoustic waves to manipulate the diffraction of light within a transparent crystal. These versatile devices are employed in various fields, such as ground- and space-based spectroscopy [1, 2] and network applications [3]. AOTFs are compact solid-state devices that filter desired optical wavelengths by applying an appropriate Radio-Frequency (RF) signal. Their compactness, robustness and quick tunability enables fast, efficient, and precise control over the spectral properties of light. AOTFs allow for the selective transmission or blocking of specific optical wavelengths, which makes them particularly appealing for space-based missions [4].
To operate AOTFs and regulate light diffraction at a specific optical wavelength, a transducer is mounted to the side of a transparent crystal, such as TeO_2 or quartz. This transducer converts RF signals of a designated frequency and power into sound waves [5]. Applying the appropriate frequency and power level, the Bragg matching condition can be satisfied, enabling two first-order diffracted light beams emitting at the crystal's output [6].
Using commercial off-the-shelf (COTS) AOTFs in an optical setup comes with certain challenges. Mostly the information provided on critical parameters in order to have an optimal functioning AOTF, is limited.
The aim of this paper is to present an optimization algorithm, using an analytical model, in order to characterize the AOTF's crystallographic axis angle θ_c, the tilt-angle α, as well as facet inclination angles β and γ (Fig. 1). Therefore, first a diffraction testing is done using

[*] ***Corresponding author***: *j.a.m.vanhamel@tudelft.nl*

a COTS AOTF working in the optical visible domain. Both output ray angles are recorded, together with the momentum-matching frequency. Additionally, a developed optimization algorithm is applied to the analytical model, providing the parameters θ_c, α, γ, and β.

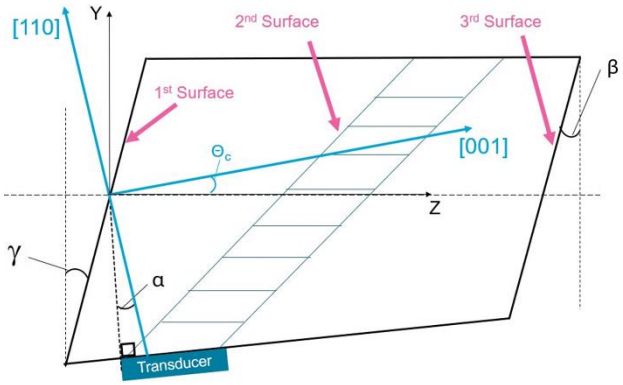

Figure 1. AOTF setup and positioning of the global (black) and crystallographic (blue) coordinate systems.

2. AOTF PARAMETER CHARACTERIZATION APPROACH

The optimization algorithm requires the analytical model's outputs in order to find optimal values that can characterize the main AOTF angles.. First, this model is briefly explained, followed by experimental diffraction tests. Consequently, the algorithm is applied to the model and the AOTF characterization parameters are obtained.

2.1 Analytical model

The goal of the analytical model is to provide as an output the undiffracted ray's optical path through the AOTF, as well as ray tracing of the diffracted ray, accompanied with the frequency signal required for the momentum-matching condition.

The model is based on the approach proposed by Zhao et al. [7], where the AOTF is split into three different surfaces, namely the AOTF entrance surface, the acoustic field and the exit surface (see Fig. 1). Using Directional Cosine Matrices (DCM) in 3D provides the baseline for the Python-based analytical model used in this research. This model has been broken down into more substages and uses adapted mathematical expressions in comparison to Zhao et al. [7], allowing a broad range of optical wavelengths in which the model is applicable.

2.2 Experimental diffraction tests

In this section, diffraction testing on a TeO_2 COTS AOTF (550 – 1000 nm) was carried out by recording both output ray angles, the rotational angle of the AOTF and the momentum-matching frequency. A vertically polarized 635 nm laser light is applied to the AOTF via a polarizer and an iris (Fig. 2). The diffraction occurred only when a vertically polarized light was shone, using a 145 MHz RF signal applied to the AOTF transducer. This RF signal was generated using a lab RF generator and amplifier setup.

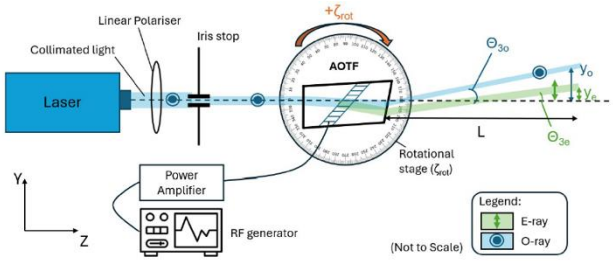

Figure 2. AOTF diffraction test setup with ζ_{rot} is the rotational angle, θ_{3o} is the ordinary undiffracted ray angle and θ_{3e} is the extraordinary diffracted ray.

An example of this diffraction is shown in Fig. 3, where the diffracted light appears faint to the left of the undiffracted light. The dimness of the diffracted light is due to the RF power being set at 100 mW.

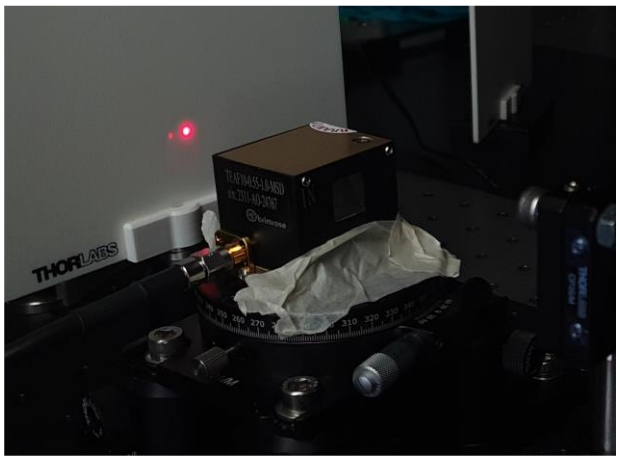

Figure 3. AOTF diffraction when a vertically polarised light is shone onto the AOTF.

The momentum-matching frequency was determined, by rotating the AOTF over a limited range (from -2 degrees

to 8 degrees, compared to the incoming light beam) using the rotational stage (Fig. 2 and 3). The accompanying diffracted and undiffracted rays angles θ_{3o} and θ_{3e} were also recorded by detecting the peak diffracted ray intensity.

2.3 Algorithm selection

To integrate the developed analytical model with an optimization algorithm, the first step was to identify a suitable algorithm. The approach involved selecting an existing method and adapt the analytical model accordingly. Given that the model was implemented in Python and involved multiple variables influencing the results, the selection was limited to multi-variable optimization algorithms available in SciPy. The "L-BFGS-B" algorithm (Limited-memory Broyden-Fletcher-Goldfarb-Shanno) was chosen due to its suitability for multi-variable nonlinear problems and its computational efficiency compared to other quasi-Newton methods [8]. Moreover, this algorithm supports box constraints, allowing for straightforward boundary conditions on variables (θ_c, α, γ, β).

Quasi-Newton methods aim to find a local minimum by approximating the curvature of the objective function, focusing on values where the function approaches a local minimum [8]. To determine the curvatures for each search variable, these methods typically rely on an inverse Hessian matrix [9], containing the second-order partial derivatives. However, calculating a full Hessian becomes increasingly time-consuming as the number of variables (n) grows [10]. To address this, the limited-memory approach estimates the Hessian matrix using only recent search iterations, rather than each time recalculating it from scratch [10]. A detailed mathematical explanation of how this algorithm works is beyond the scope of this research. The primary reason for selecting this algorithm is its computational efficiency in solving multi-variable problems and its ease of implementation in Python through the SciPy library, which also supports simplified variable constraints. Furthermore, the algorithm is relatively effective in finding a global minimum (optimal value) of the objective function [10].

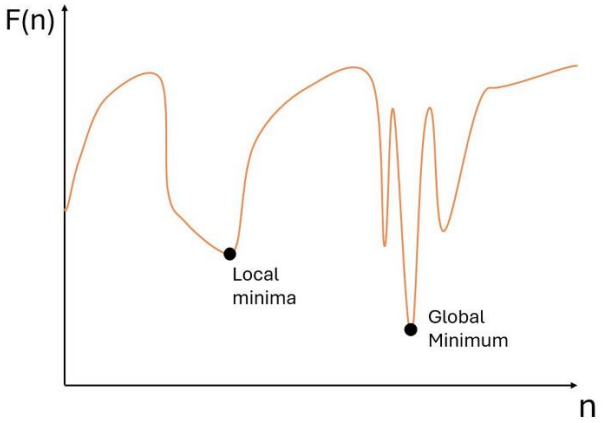

Figure 4. Simplified multimodal example where finding global minimum is challenging for Newton methods.

However, L-BFGS-B can become trapped in local minima, as shown in Fig. 4. This is an example of an objective function with a single variable n demonstrating this limitation [10]. To address this, running the algorithm multiple times with different initial guesses can improve the chances of finding the global minimum.

In contrast, genetic algorithms are generally more effective at locating the global minimum in such cases. Nevertheless, they are more complex to implement, requiring constraints within the objective function, and often come with higher computational costs [11, 12]. Due to these factors, genetic algorithms were not considered in this study but are recommended for future research.

2.4 Objective function and bounds selection

With the L-BFGS-B algorithm selected, the next step is to define its input for optimization. The primary input is the objective function — a scalar function that the algorithm seeks to minimize [10]. The objective is to reduce the discrepancy between the experimental measurements from the COTS AOTF diffraction testing and the predictions from the analytical model. This discrepancy is quantified as a total error, formulated in Eqn. 1 as the objective function. This represents the sum of squared errors for momentum-matching frequency and diffracted/undiffracted angles.

$$E_{tot} = E_{freq} + E_{diff} + E_{undiff} \quad (1)$$

Where each term is defined as follows:

$$E_{freq} = \sum_{i=1}^{n} \left(f_i^{exp} - f_i^{sim} \right)^2 \quad (2)$$

$$E_{diff} = \sum_{i=1}^{n} \left(\theta_{e,i}^{exp} - \theta_{e,i}^{sim}\right)^2 \quad (3)$$

$$E_{undiff} = \sum_{i=1}^{n} \left(\theta_{o,i}^{exp} - \theta_{o,i}^{sim}\right)^2 \quad (4)$$

In Eqn. 2, 3 and 4, *n* represents the number of data points in the experimental results array f^{exp} (momentum-matching frequency), obtained from the diffraction testing, with each point corresponding to a different ζ_{rot} angle. f^{sim} represents the simulated values of the momentum-matching frequency generated by the optimization algorithm. The squared difference is selected because it assigns greater weight to larger errors, ensuring the optimization algorithm to prioritize reducing significant discrepancies.

During each iteration, the algorithm tests different configurations of the variables θ_c, α, γ and β, aiming to minimize the cumulative error across all three equations, thus optimizing the objective function.

To ensure the search remains within realistic AOTF parameter ranges, bounds were set for θ_c, α, γ and β. The selected bounds for the COTS AOTF are listed in Tab. 1, where the left is the lower bound, and the right is the upper bound.

Table 1. Optimization variables and their bounds.

Variable	Bounds	Unit
θ_c	[10; 55]	Degrees
α	[5; 16]	Degrees
γ	[-0.1; 0.1]	Degrees
β	[5; 12]	Degrees

3. EVALUATION OF THE OPTIMIZATION RESULTS

After setting the objective function and bounds for the L-BFGS algorithm, the optimization was executed multiple times with varying initial guesses to avoid the algorithm from becoming stuck in a local minimum. Each optimization run converged to the optimized parameters listed in Tab. 2.

Table 2. Optimized parameters.

Variable	Optimized value	Unit
θ_c	25.92	Degrees
α	11.97	Degrees
γ	-0.1	Degrees
β	7.2	Degrees

The optimized values were subsequently applied to the analytical model. A frequency matching graph is shown in Fig. 5, indicating the match between the predictions (in green) and the experimentally obtained data (in blue). It can be seen that the frequency remains relatively consistent as the rotational angle increases.

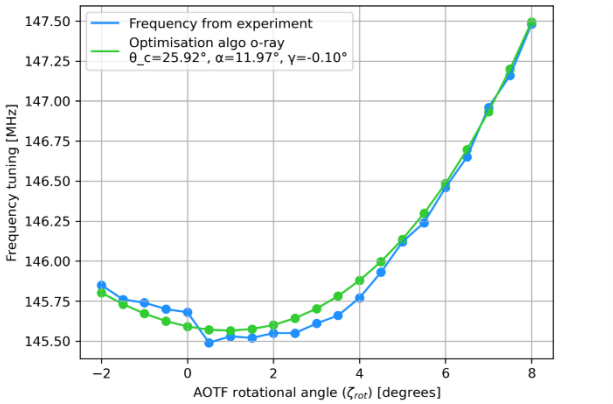

Figure 5. Momentum-matching frequencies as a function of AOTF rotational angle for the ordinary ray diffraction test.

The undiffracted and diffracted angle results are considered together. For the undiffracted rays presented in Fig. 6, in which β plays a key role, the optimization algorithm slightly overestimates the experimental curve.

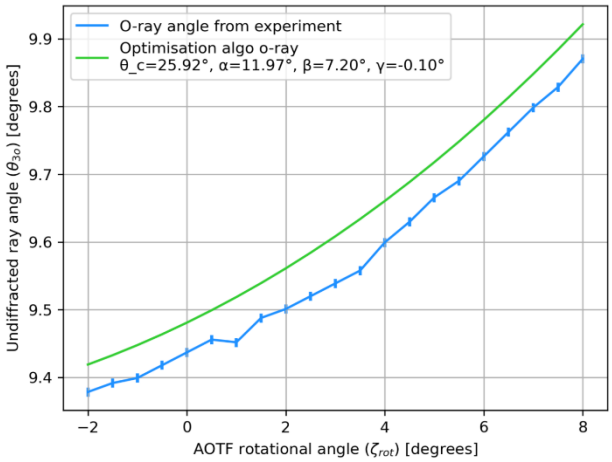

Figure 6. Undiffracted ray angles (θ_{3o}) as a function of AOTF rotational angle for the o-ray diffraction test.

Notably, the angles of the diffracted rays remain extremely stable for this AOTF, consistently ranging between 2.65° and 2.70° (Fig. 7). This stability is an advantage for the optical design, enabling precise predictions of the diffracted ray's path and accurate CCD placement. However, this stability also creates a challenge for the optimization algorithm. When the algorithm attempts to reduce the simulated undiffracted angle by lowering β, it inadvertently shifts the diffracted angle values downward, which penalizes the algorithm if β is reduced too much.

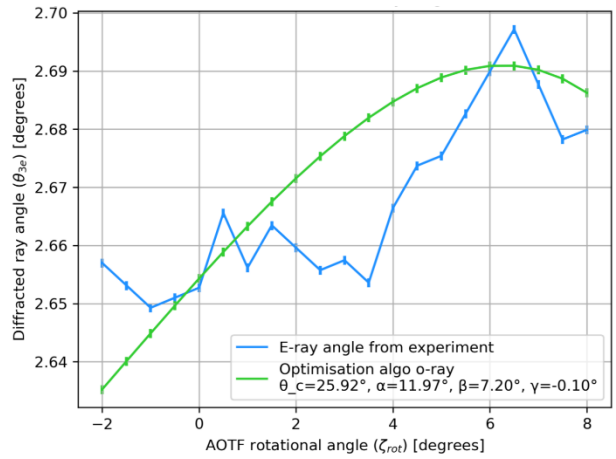

Figure 7. Diffracted ray angles (θ_{3e}) as a function of AOTF rotational angle for the o-ray diffraction test.

In general, the optimization algorithm shows good results, with all simulation curves aligning closely with the experimental data with a discrepancy between experimental and calculated values below 0,02° (Fig. 7). These frequency mismatches could arise from small deviations in the crystal's material properties, such as the acoustic velocity or refractive indices, compared to the values used in the analytical model.

4. CONCLUSIONS

In this research, a dedicated optimization algorithm is explored, in combination with an analytical model. The goal is to find characterization parameters linked to the practical build of the AOTF. The results show that the unknown parameters θ_c, α, γ, and β can be determined.
The L-BFGS optimization algorithm was selected due to its efficiency in handling multiple variables, its computational speed, and its enhanced capability in locating global minima compared to simpler optimization methods. To direct the optimization, an objective function was defined in order to minimize the difference between the simulated and measured values. Additionally, search bounds were set for the AOTF parameters θ_c, α, γ, and β, constraining the algorithm's variable adjustments within these limits.
The optimized values for these four parameters generated curves that closely matched the experimental results. Further improvements could be achieved by either adjusting the penalty in the objective function to refine frequency-matching curves or by incorporating additional variables, such as the material's acoustic velocity. These changes would increase computational time due to the added search variables, but could enhance the characterization process.

5. ACKNOWLEDGMENTS

The authors would like to thank the Delft University of Technology (TU Delft) and the l'Université Polytechnique Hauts-de-France (UPHF), to accommodate this collaboration and experimental work.

6. REFERENCES

[1] E. Dekemper, J. Vanhamel, B. Van Opstal, and D. Fussen, "The AOTF-based NO2 camera," *Atmospheric Measurement Techniques*, vol. 9, no. 12, pp. 6025-6034, 2016.

[2] J. Li, Y. Gui, R. Xu, Z. Zhang, W. Liu, G. Lv, M. Wang, C. Li,and Z. He: "Applications of Aotf

Spectrometers in in Situ Lunar Measurements," *Materials*, vol. 14, no. 13, pp. 3454-, 2021.

[3] C.S. Sobrinho, M.V.N. De Oliveira, M.G. Da Silva, J.L.S. Lima, E.F. De Almeida, and A.S.B. Sombra: "Numerical Analysis of the Crosstalk on an Integrated Acousto-Optic Tunable Filter (AOTF) for Network Applications," *Fiber and Integrated Optics*, vol. 23, no. 5, pp. 345–363, 2004.

[4] O.I. Korablev, A.Yu. Trokhimovskiy, Yu.K. Kalinnikov, "AOTF spectrometers in space missions and their imaging capabilities," in *International Conference on Space Optics ICSO 2016*, (Biarritz, France), pp. 105621M-1-8, 2016.

[5] A.P. Goutzoulis and D.R. Pape: *Design and Fabrication of Acousto-Optic Devices*, New York-Basel-Hong Kong: Marcel Dekker, Inc., 1994.

[6] T. Yano, and A. Watanabe: "Acoustooptic TeO_2 tunable filter using far-off-axis anisotropic Bragg diffraction," *Appl. Opt.*, vol. 15, pp. 2250-2258, 1976.

[7] H. Zhao, C. Li, and Y. Zhang: "Three-surface model for the ray tracing of an imaging acousto-optic tunable filter," *Appl. Opt.*, vol. 53, no. 32, pp. 7684–7690, 2014.

[8] K. Kumar, D. Ghosh, A. Upadhayay, J. Yao, X. Zhao, and A. Upadhyay: "Quasi-newton methods for multiobjective optimization problems: A systematic review," *Applied Set-Valued Analysis and Optimization*, vol. 5, no. 2, pp. 291–321, 2023.

[9] A. Sadeghi-Lotfabadi, and K. Ghiasi-Shirazi, "Speeding up L-BFGS by Direct Approximation of the Inverse Hessian Matrix," *Computational Optimization and Applications*, 2025.

[10] T.V. Mikosch, S.I. Resnick, and S.M. Robinson: *Numerical Optimization*, Springer Series in Operations Research and Financial Engineering. New York, Springer Science+Business Media, LLC, 2006.

[11] G.G. Wang and A.H. Alavi: *Evolutionary Computation*. Basel: MDPI, 2019.

[12] T.E.B. Davies, D.P. Mehta, J.L. Rodríguez-López, G.H. Gilmer, and C. V. Ciobanu: "A Variable-Number Genetic Algorithm for Growth of 1-Dimensional Nanostructures into Their Global Minimum Configuration Under Radial Confinement," *Materials and Manufacturing Processes*, vol. 24, no. 3, pp. 265-273, 2009.